J Membrane Biol (2016) 249:381–391
DOI 10.1007/s00232-016-9876-3

The Location of the Protonated and Unprotonated Forms of Arbidol in the Membrane: A Molecular Dynamics Study

Vicente Galiano[1] · **José Villalaín**[2]

Received: 5 October 2015 / Accepted: 24 January 2016 / Published online: 3 February 2016

Abstract Arbidol is a potent broad-spectrum antiviral molecule for the treatment and prophylaxis of many viral infections. Viruses that can be inhibited by arbidol include enveloped and non-enveloped viruses, RNA and DNA viruses, as well as pH-independent and pH-dependent ones. These differences in viral types highlight the broad spectrum of Arb antiviral activity and, therefore, it must affect a common viral critical step. Arbidol incorporates rapidly into biological membranes, and some of its antiviral effects might be related to its capacity to interact with and locate into the membrane. However, no information is available of the molecular basis of its antiviral mechanism/s. We have aimed to locate the protonated (Arp) and unprotonated (Arb) forms of arbidol in a model membrane system. Both Arb and Arp locate in between the hydrocarbon acyl chains of the phospholipids but its specific location and molecular interactions differ from each other. Whereas both Arb and Arp average location in the membrane palisade is a similar one, Arb tends to be perpendicular to the membrane surface, whereas Arp tends to be parallel to it. Furthermore, Arp, in contrast to Arb, seems to interact stronger with POPG than with POPC, implying the existence of a specific interaction between Arp, the protonated from, with negatively charged phospholipids. This data would suggest that the active molecule of arbidol in the membrane is the protonated one, i.e., the positively charged molecule. The broad antiviral activity of arbidol would be defined by the perturbation it exerts on membrane structure and therefore membrane functioning.

Graphical Abstract

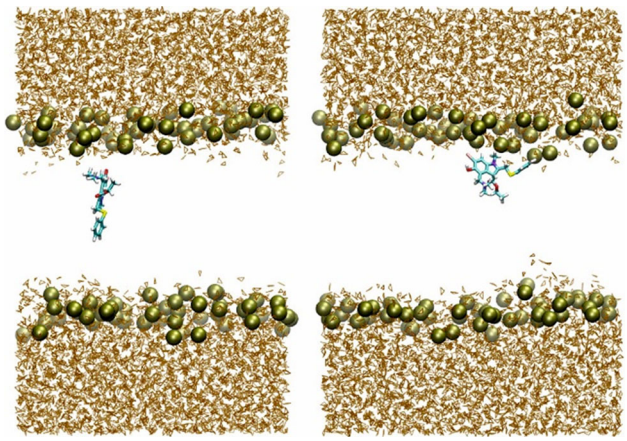

Keywords Arbidol · Molecular dynamics · Membrane location

Abbreviations

Chol	Cholesterol
Arb	Arbidol (un-protonated form)
Arp	Arbidol (protonated form)
POPC	1-Palmitoyl-2-oleoyl-sn-glycero-3-phosphocholine
POPG	1-Palmitoyl-2-oleoyl-sn-glycero-3-phospho-(1′-rac-glycerol)

Electronic supplementary material The online version of this article (doi:10.1007/s00232-016-9876-3) contains supplementary material, which is available to authorized users.

✉ José Villalaín
jvillalain@umh.es

[1] Physics and Computer Architecture Department, Universitas "Miguel Hernández", 03202 Elche-Alicante, Spain

[2] Molecular and Cellular Biology Institute, Universitas "Miguel Hernández", 03202 Elche-Alicante, Spain

Introduction

Arbidol is a potent broad-spectrum antiviral molecule clinically approved in Russia for the treatment and prophylaxis of acute respiratory infections, including influenza A and B infections (Boriskin et al. 2008). Arbidol is also licensed for the treatment of rotavirus infection. Viruses that can be inhibited by arbidol include enveloped and non-enveloped viruses, RNA and DNA viruses, as well as pH-independent and pH-dependent ones. Arbidol therefore exhibits a broad and potent antiviral activity against a number of viruses which include viruses such as adenovirus, avian coronavirus, avian viruses, Chikungunya virus, Coxsackie virus B5, Hantaan virus, hepatitis B and C viruses, infectious bronchitis virus, influenza, poliovirus, and reovirus, among others (Brooks et al. 2012; Delogu et al. 2011; Deng et al. 2009; Liu et al. 2013; Perfetto et al. 2014; Shi et al. 2007; Zhong et al. 2009). Very recently other viruses such as Ebola virus, Tacarive arenavirus and human herpes virus 8 have been also shown to be inhibited in vitro by Arbidol (Pecheur et al. 2016). These differences in viral types undoubtedly highlight the broad spectrum of arbidol antiviral activity as well as that it must affect a common critical step in viral entry, fusion, and/or replication.

The chemical name of arbidol is ethyl-6-bromo-4-[(dimethylamino)methyl]-5-hydroxy-1-methyl-2-[(phenylthio)methyl]-indole-3-carboxylate (Fig. 1), is relatively well-tolerated, is highly soluble in organic media because of its hydrophobicity, and incorporates rapidly into model and biological membranes (Teissier et al. 2011b; Villalain 2010). It has been found previously that arbidol displays interfacial properties in membranes and intercalates in the phospholipid palisade structure of the membrane (Teissier et al. 2011b; Villalain 2010). Interestingly, arbidol interaction with membranes is more pronounced at acidic pH, i.e., the pH required for the crucial fusion step of several enveloped viruses (Pecheur et al. 2007; Teissier et al. 2011a). The molecule of arbidol has the capacity of forming hydrogen bonds with phospholipid molecules, having four possible acceptor groups and one possible donor group. At the same time, arbidol is a weak base which could be protonated when inserted in the membrane giving place to a positively charged molecule (Fig. 1) (Boriskin et al. 2008; Pecheur et al. 2007). Therefore, arbidol could be present in the membrane in two different species, protonated (Arp), and un-protonated (Arb). Arb/Arp interacts and modifies the physico-chemical properties of membrane phospholipids, more significantly on negatively charged phospholipids than on zwitterionic ones, suggesting that the active molecule of arbidol in the membrane is the protonated one, i.e., the positively charged molecule (Villalain 2010). Therefore, Arb/Arp could perturb membrane structure depending on the relative proportion of the protonated and un-protonated forms in the membrane.

It has been also found that Arb/Arp increases the stability of influenza virus hemagglutinin as well as with other viral proteins; it is then possible that Arb/Arp, apart from interacting with biomembranes, also interacts with viral envelope proteins (Leneva et al. 2009; Nasser et al. 2013). Arb has been shown to inhibit chikungunya hemagglutination, suggesting that Arb/Arp interferes with the replication cycle (Delogu et al. 2011). Arb/Arp even might have an immune-stimulating effect (Blaising et al. 2014). Arb/Arp acts via hydrophobic interactions with the cell membrane as well as through interaction with viral proteins inhibiting both viral fusion and viral entry into the cell. Furthermore, several viruses modulate lipid metabolism and modify the internal membrane environment to favor viral replication. (Blaising et al. 2014; Boriskin et al. 2008; Teissier et al. 2011a, b; Villalain 2010). Therefore, Arb/Arp could interact with membrane phospholipids, bind specific cellular, and/or viral proteins as well as could impair the formation of the membranous web necessary for viral replication.

In this work, we have used molecular dynamics to discern the location and orientation of Arb/Arp in model membranes. Molecular dynamics can be used to probe the dynamics, interaction, structure, and location of different types of molecules inserted in biological model membranes (Ingolfsson et al. 2014). The fact that Arb/Arp mode of action is most likely through membrane interaction, it seems reasonable to think that its mode of action might be at least partly attributable to its specific effect on the membrane structure, its specific interactions with particular lipid molecules and, last but not least, its location and orientation inside the membrane. Therefore, we have used a model membrane composed of two different phospholipids, a zwitterionic one, 1-palmitoyl-2-oleoyl-sn-glycero-3-phosphocholine (POPC) and a negatively charged one, 1-palmitoyl-2-oleoyl-sn-glycero-3-phospho-(1′-rac-glycerol (POPG). Our results support an interfacial location of Arb/Arp in the membrane, the existence of specific interactions with phospholipids and interestingly, Arb and Arp orientate differently in the membrane, facts that could explain, at least in part, some of its very interesting biological effects.

Materials and Methods

Molecular Dynamics Simulation

Unrestrained all-atom molecular dynamics simulations were carried out using NAMD 2.9 (Phillips et al. 2005) utilizing the CHARMM36 force field for the lipid molecules (Klauda et al. 2010) and the CHARMM general force field for Arb/Arp (Vanommeslaeghe et al. 2010) (http://mackerell.

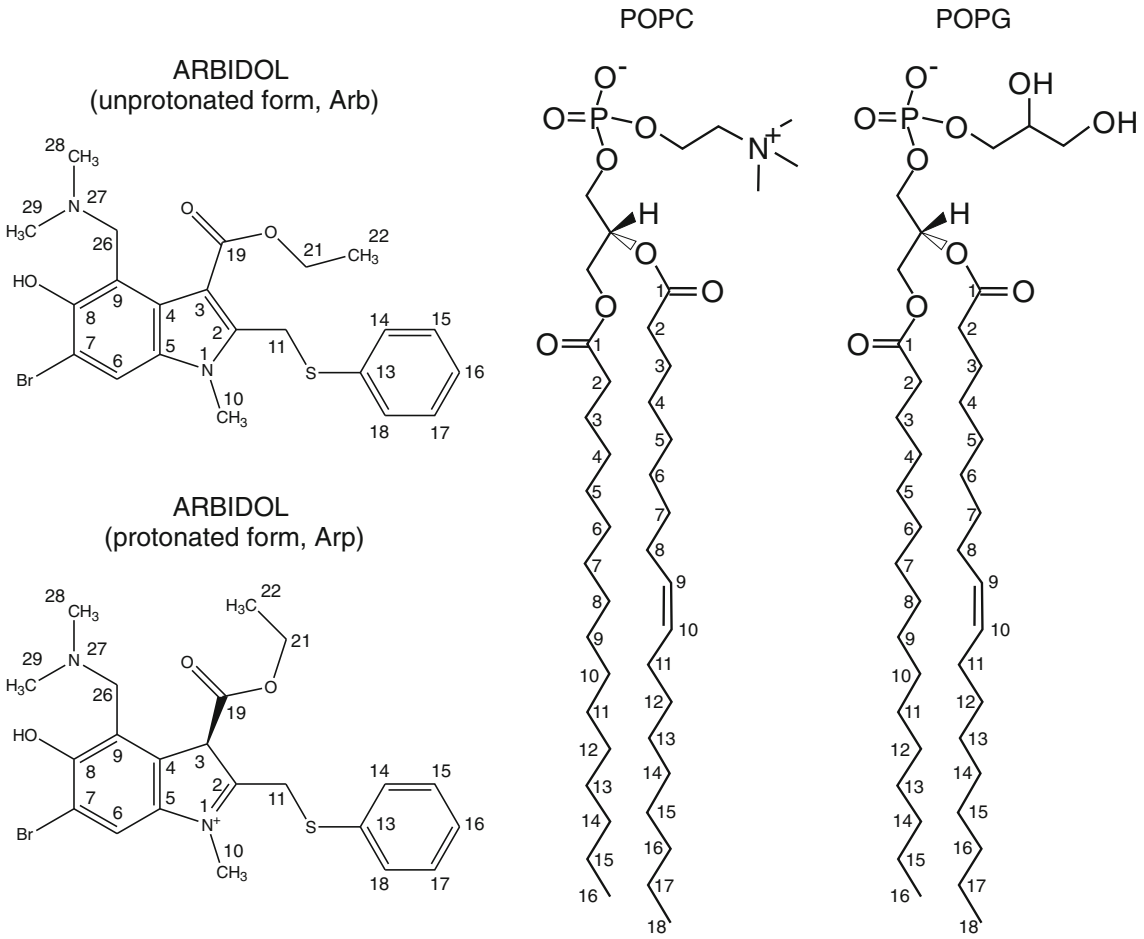

Fig. 1 Molecular structures of arbidol (ethyl-6-bromo-4-[(dimethylamino)methyl]-5-hydroxy-1-methyl-2-[(phenylthio)methyl]-indole-3-carboxylate) in its unprotonated (Arb) and protonated (Arp) forms as well as POPC (1-palmitoyl-2-oleoyl-sn-glycero-3-phosphocholine) and POPG (1-palmitoyl-2-oleoyl-sn-glycero-3-phospho-(1′-rac-glycerol)). Numbering of particular atoms mentioned in the text is also given. Hydrogens have been omitted for clarity

umaryland.edu/charmm_ff.shtml). The TIP3P model was used for water (Ozu et al. 2013). All simulations were carried out with a constant number of particles as an NPT ensemble at 1.0 atm and 310 K. The time step was 2 fs. Constant pressure was maintained by the Nosé-Hoover Langevin piston method (Feller et al. 1995; Martyna et al. 1994). Constant temperature was maintained by Langevin dynamics with a damping coefficient γ of 0.5 ps^{-1}. The standard particle mesh Ewald method was used with periodic boundary conditions to calculate the long-range electrostatic interaction of the systems. Non-bonded interactions were cut-off after 12 Å with a smoothing function applied after 10 Å (Patra et al. 2003). Prior to simulation and in order to remove unfavorable atomic contacts, the membrane model systems were previously equilibrated for 1 ns after 50,000 steps of minimization. The production trajectory of the lipid systems was calculated for 175 ns. All simulations were conducted under electrostatically neutral environment with an appropriate number of sodium ions.

Bilayer Membrane Model

We have used a lipid bilayer model composed of 128 lipid molecules (64 lipids in each leaflet) in a rectangular box. It was comprised 16 molecules of cholesterol, 80 molecules of POPC, and 32 molecules of POPG surrounded by 5559 molecules of water. Thus the relationship POPC/POPG/Chol was 5:2:1. The solvent-to-lipid ratio was ~43, i.e., excess water (Murzyn et al. 2001). Figure 1 presents the structures and carbon numbering of the molecules considered in this study, the un-protonated form of arbidol, Arb, the protonated from of arbidol, Arp, POPC, and POPG. The bilayer lied in the *xy* plane, and the bilayer normal was parallel to the *z*-axis. Initially the simulation box had the dimensions of 8.9 nm in the *x*- and *y*-directions and 8 nm in the *z*-direction. The height of the simulation box and the cross-sectional area were allowed to vary independently of each other. Each water layer had an average dimension of 5.4 Å between membranes due to periodic boundary

conditions. Arb/Arp was generated and minimized using Discovery Studio 4.0 software (Accelrys Inc., San Diego, USA). As it is well known, phosphatidylcholine is the dominant lipid species in biological membranes, cholesterol is omnipresent in many types of membranes giving them unique biophysical properties, and phosphatidylglycerol provides negative charge at the membrane surface (van Meer et al. 2008). From the negatively charged diacylglycerol-phospholipids that could be selected, i.e., PA, PG, and PS, we have chosen PG. PG's have almost identical phase transition properties as zwitterionic PC's with the same length fatty acid chains. Moreover, PG's are one of the most studied negatively charged phospholipids by biophysical methods. PA, similarly to PG, has one negative charge but its biophysical properties are significantly different. PS, in contrast to both PG and PA, has three charges, two negative and one positive, and its biophysical properties, compared to PC, are different. Being POPC and POPG the phospholipid molecules used in this work, the palmitoyl chain located in the sn-1 position is completely saturated, whereas the oleoyl chain located in the sn-2 position contains a cis double bond between the C9 and C10 carbons (see Fig. 1 for acyl chain numbering). The presence of the oleoyl chain in the sn-2 position increases the overall mobility of the hydrocarbon chains of the phospholipids and hence fluidity in the xy plane of the membrane. The lipid membrane models, including water, POPC, POPG, and cholesterol, were prepared using the Charmm-Gui web server (http://www.charmm-gui.org, Wu et al. 2014). ParamChem (https://cgenff.paramchem.org, Vanommeslaeghe et al. 2010) was used to obtain the CHARMM general force field (CGenFF) compatible stream file of Arb/Arp which contained the optimized parameter and topology data of the molecule (for the optimization guide see http://mackerell.umaryland.edu/~kenno/cgenff/). The automatic PSF generation plugin for VMD (Humphrey et al. 1996) utilized the Arb/Arp stream file data to obtain the psf and pdb files of Arb/Arp required by VMD/NAMD to build the complete system. Since Arb/Arp have a highly hydrophobic character and a high phospholipid/water partition coefficient (Villalain 2010), at the beginning of the simulation the Arb/Arp molecules were embedded at the center of the lipid bilayer in order to quickly reach convergence (Galiano and Villalain 2015; Kosinova et al. 2012).

Data Analysis

The surface of the membrane was defined by the layer of the phosphate atoms of the phospholipid headgroups and were oriented parallel to the *xy* plane. Bilayer thickness was defined as the average distance between the phospholipid phosphorus atoms of the opposing leaflets, whereas the center of the bilayer, $z = 0$, was defined by the center-of-mass of the phosphate atoms of the phospholipid molecules. The center-of-mass *z*-distance of the Arb/Arp molecule relative to the center of the bilayer was used to study its spatial distribution in the membrane. The Arb/Arp membrane relative orientation was measured by the angle defined by the *z*-axis and the vector defined by carbons C4 and C4′ of the molecule of Arb/Arp (see Fig. 1 for numbering). The analysis was performed over the whole MD simulation unless stated otherwise. VMD (Humphrey et al. 1996) and Pymol were used for visualization and analysis. SCD order parameters, membrane thickness, molecular areas, center-of-mass, and molecule tilt were obtained using VMD Membplugin (Guixa-Gonzalez et al. 2014), whereas the mass density profiles were obtained using the VMD Density Profile Tool plugin (Giorgino 2014).

Results and Discussion

We have used the time variation of the area per lipid as an indicator of the equilibration of the bilayer and its average value to assess the adequacy of the simulation methodology (Anézo et al. 2003; Kandt et al. 2007). The time traces of the area per molecule for the system POPC/POPG/Chol/Arb corresponding to the z+ and z− leaflets are shown in Fig. S1A and S1C, respectively. As expected, no significant changes were found in the general bilayer properties in this diluted system, i.e., system having 128 lipid molecules and only 1 molecule of Arb. The data show that phospholipids and cholesterol were equilibrated early on the course of the simulation, either at the z+ or at the z− bilayer leaflets, indicating that the system reached a steady state after 1500 ps of simulation. The time traces of the molecular area for the system POPC/POPG/Chol/Arp and corresponding to the z+ and z− leaflets are shown in Fig. S1B and S1D, respectively. As commented above, no significant changes were found in the general properties in this diluted system, and the phospholipid and cholesterol molecules were equilibrated at both leaflets early on the course of the simulation time. In this case, the system reached a steady state after 2000 ps of simulation. At the end of both simulations, one system containing Arb and the other containing Arp, the mean area of POPC, POPG, and Chol were 58–60, 59–62, and 27–33 A^2, respectively, in agreement with previously reported data (Zhuang et al. 2014).

In contrast, the molecular area of either Arb or Arp were different from those of the phospholipids and cholesterol and at the same time, and they differed from each other (Fig. S1A and S1B). Furthermore, the molecular area of both Arb and Arp presented a great variation along the whole simulation time in each membrane model system. This variation in molecular area should be due to differences in membrane location, molecule orientation, or both.

Apart from that, comparing the molecular areas of Arb (Fig. S1A) and Arp (Fig. S1B), it is possible to see that Arb variation was greater than the Arp one. Whereas the molecular area of Arb along the whole simulation time oscillated between 30 and 105 A^2, i.e., a difference of about 75 A^2, the molecular area of Arp oscillated between 60 and 110 A^2, i.e., a difference of about 50 A^2. The area histograms for Arb and Arp for the last 2 ps of the simulation are shown in Fig. S1E and S1F, respectively. The mean area of Arb was found to be about 65–70 A^2, whereas the mean area of Arp was about 80 A^2. The area dispersion was lower for Arb, about 30 A^2, than for Arp, about 45 A^2.

The time variation of the center-of-mass for both Arb and Arp molecules compared with the z+ phosphate atoms center-of-mass are shown in Fig. 2a, b, respectively. Arb equilibrated to a position similar to that found at the end of the simulation in about 40 ns, although there was a noticeable dispersion in the center-of-mass variation of the molecule along the whole simulation time. It had a minimum of about 4 Å and a maximum of about 17 Å, i.e., a variation of about 12 Å (Fig. 2a). The time needed by Arp to reach a quasi-equilibrium position was significantly lower than Arb, since it was reached at about 2 ns (Fig. 2b). The center-of-mass dispersion of Arb was also significantly lower than Arb, since along the whole simulation time it varied from about 8–17 Å. The histograms corresponding to the Arb and Arp center-of-mass for the last 2 ps of the simulation are shown in Fig. 2c, d, respectively. There was a small difference in the final location of the center-of-mass of both molecules, since that pertaining to Arb was located at about 10–11 Å from the center of the bilayer, whereas that corresponding to Arp was located at about 12.5–13.5 Å. The center-of-mass dispersion was larger for Arb, about 6 Å, than for Arp, about 3.5 Å. In a similarly way to the behavior of the area versus time trend commented above, membrane thickness, measured as the average distance between the center-of-mass of the phosphate atoms of opposite leaflets, was held relatively constant after 12 and 20 ns for the systems POPC/POPG/Chol/Arb and POPC/POPG/Chol/Arp, respectively (Fig. 2e, f). These data would indicate again a rapid equilibration of both systems.

The orientation of both Arb and Arp in the membrane was studied considering the angle formed by the vector joining ring carbons 9 and 16 of Arb/Arp with the membrane *z*-axis (Fig. 3, scheme). There was a great deviation in angle for Arb along the simulation time, since the highest observed angle was about 175° and the lowest one was about 2° (Fig. 3a). This is in contrast with the angle variation observed for Arp, where the angle values ranged from a minimum value of about 39° and a maximum of 135° (Fig. 3b). At the end of the simulation, the dispersion was a bit lower for Arb than for Arp (Fig. 3c). For the last 2 ns, Arb presented an average angle of about 155–160° ± 20°, whereas Arp presented an average angle of about 80° ± 20° (Fig. 3c), indicating a significant difference in molecular orientation between Arb and Arp in the membrane (see below).

We have analyzed a different but related parameter concerning the molecular orientation of both Arb and Arp in the membrane, i.e., the difference between the *z*-axis values of carbon 16 and nitrogen 27 (Fig. 3, scheme). If the difference is 0 Å, the molecule lies nearly parallel to the membrane, if the difference approximates to 12 Å, the molecule lies nearly perpendicular to the membrane. As observed in Fig. 3d, there was a great variation in this parameter along the whole range of the simulation for Arb, ranging from 0 Å (lowest value, parallel to the membrane) to near 11.9 Å (largest value, perpendicular to the membrane). For the last 2 ns, Arb presented an average difference distance of about 10.5–11 ± 1 Å (Fig. 3f). In this way and for the last 2 ns of simulation, Arb was nearly perpendicular to the plane of the membrane. For Arp, the variation for this parameter (Fig. 3e) was lower along the whole range of the simulation than that observed for Arb, since varied from 0 Å (parallel) to near 9.7 Å (nearly perpendicular). However, Arp presented an average difference distance for the last 2 ns of about 3.5–4 ± 3.5 Å (Fig. 3f), indicating that Arp was laid in a near parallel orientation to the membrane plane for the last 2 ns. It should be taken into account that Arb/Arp have two rings and a relatively rigid structure. Furthermore, the molecule does not completely span the leaflet of the bilayer.

Another parameter we have studied which can give us a useful information about the global structure of both Arb/Arp is the distance between the farthest atoms of the molecule, i.e., nitrogen 27 and carbon 16 (Fig. 3, scheme). If the difference tends to be 0 Å, there is a twist in the molecule so that both ends tend to be next to each other; on the other way, if the difference tends to be about 12 Å, the molecule is in a complete extended configuration. As observed in Fig. 3g, the average distance between atoms 16 and 27 of Arb varied from about 9 Å to about 12 Å along the whole simulation time, whereas for Arp (Fig. 3h) the average distance between these atoms varied from about 8 Å to about 11 Å. For the last 2 ns of the simulation, the two ends of Arb presented a distance of about 11 ± 1 Å, whereas it was about 9.75 ± 1 Å for Arp (Fig. 3i). These data show us that Arb presented a nearly extended conformation, whereas Arp presented a small kink, which slightly approached the two ends of the molecule.

Mass density profiles for the model systems composed of POPC/POPG/Chol/Arb and POPC/POPG/Chol/Arp are shown in Fig. 4a, b, respectively. As seen in Fig. 4a, Arb is located at a lower depth than the phosphate groups of both phospholipids, POPC and POPG, reaching as low as the center of the bilayer, where the cholesterol tail is located. However, Arp, being located at a lower depth than the

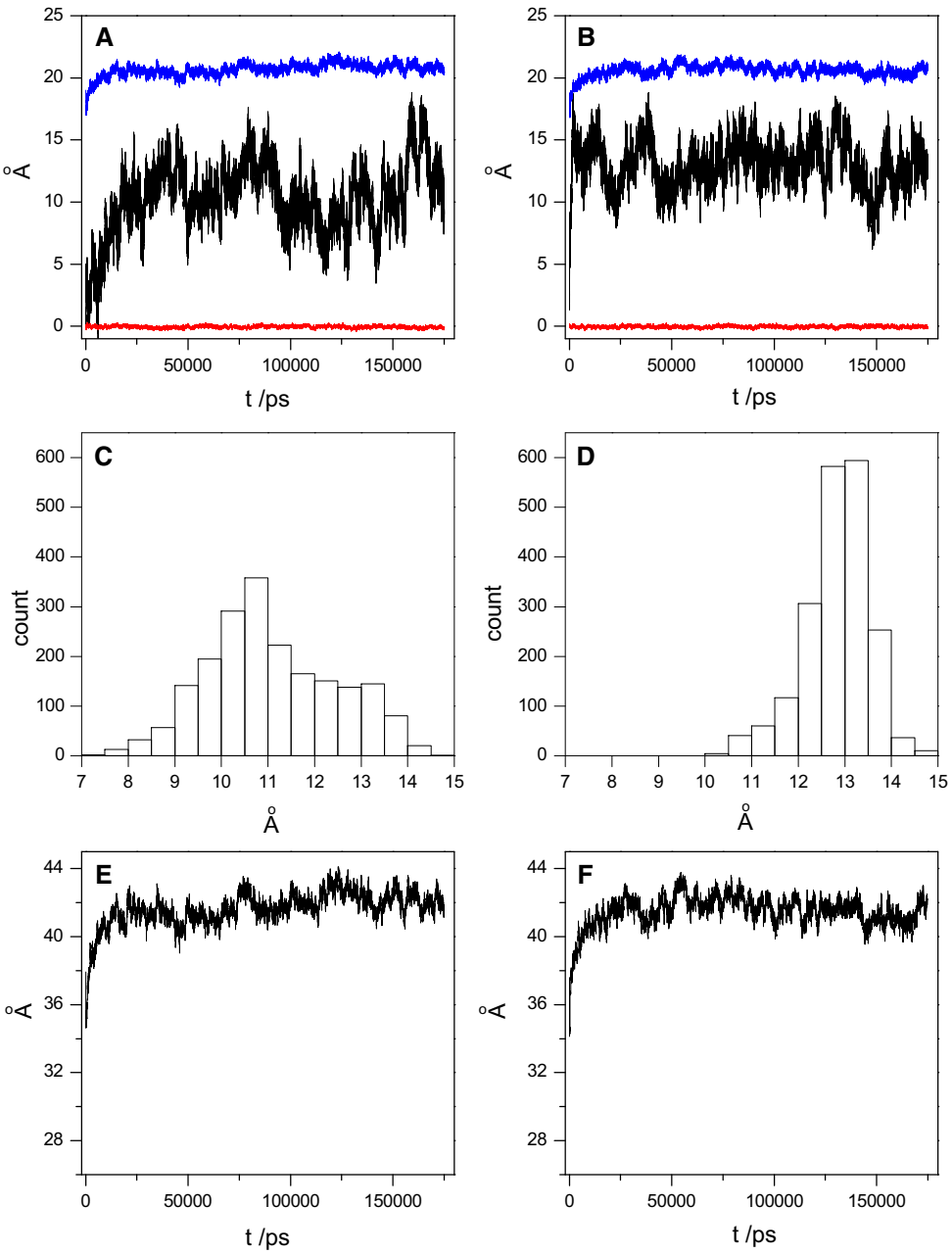

Fig. 2 Time variation of the center-of-mass of Arb and Arp for the membrane systems containing **a** POPC/POPG/Chol/Arb and **b** POPC/POPG/Chol/Arp, respectively. The average center-of-mass of Arb/Arp (*black*), the z+ leaflet phosphate atoms (*blue*), and the z+/z− leaflets phosphate atoms (*red*) are visible. The last 2 ps histograms of Arb and Arp center-of-masses are shown in **c** and **d**, respectively. The total membrane thickness for the POPC/POPG/Chol/Arb and POPC/POPG/Chol/Arp are shown in **e** and **f**, respectively (Color figure online)

phosphate groups of both phospholipids, has a membrane depth similar to that of the OH group of cholesterol (Fig. 4b). The mass density profile of the phospholipid phosphate atoms in both systems was rather symmetric. In the case of the POPC/POPG/Chol/Arb system, the half bandwidths were about 5.7 and 5.9 Å for the z+ and z− leaflets, respectively. For the POPC/POPG/Chol/Arp system, the half bandwidths were of about 5.8 and 5.2 Å for the z+ and z− leaflets, respectively. However, there were significant differences in the mass density profile of the phosphate atoms in both systems for each type of phospholipid, i.e., POPC and POPG. For the POPC/POPG/Chol/Arb system (Fig. 4c), the maximum of the POPC phosphate atoms mass density was found at 21.47 and 20.98 Å for the z+ and z− leaflets, respectively, whereas for the POPG phosphate atoms they were 20.93 and 20.48 Å, respectively. The difference between the POPC and POPG maxima were therefore 0.54 and 0.5 Å for the z+ and z− leaflets, respectively. For the POPC/POPG/Chol/Arp system (Fig. 4d), the maximum of the POPC phosphate atoms mass density was found at 21.38 and 21.17 Å for the z+ and z− leaflets, respectively, whereas for the POPG phosphate atoms they were 20.05 and 20.52 Å, respectively. The difference between the POPC and POPG maxima were therefore 1.33 and 0.65 Å for the z+ and z− leaflets, respectively. This data would imply the

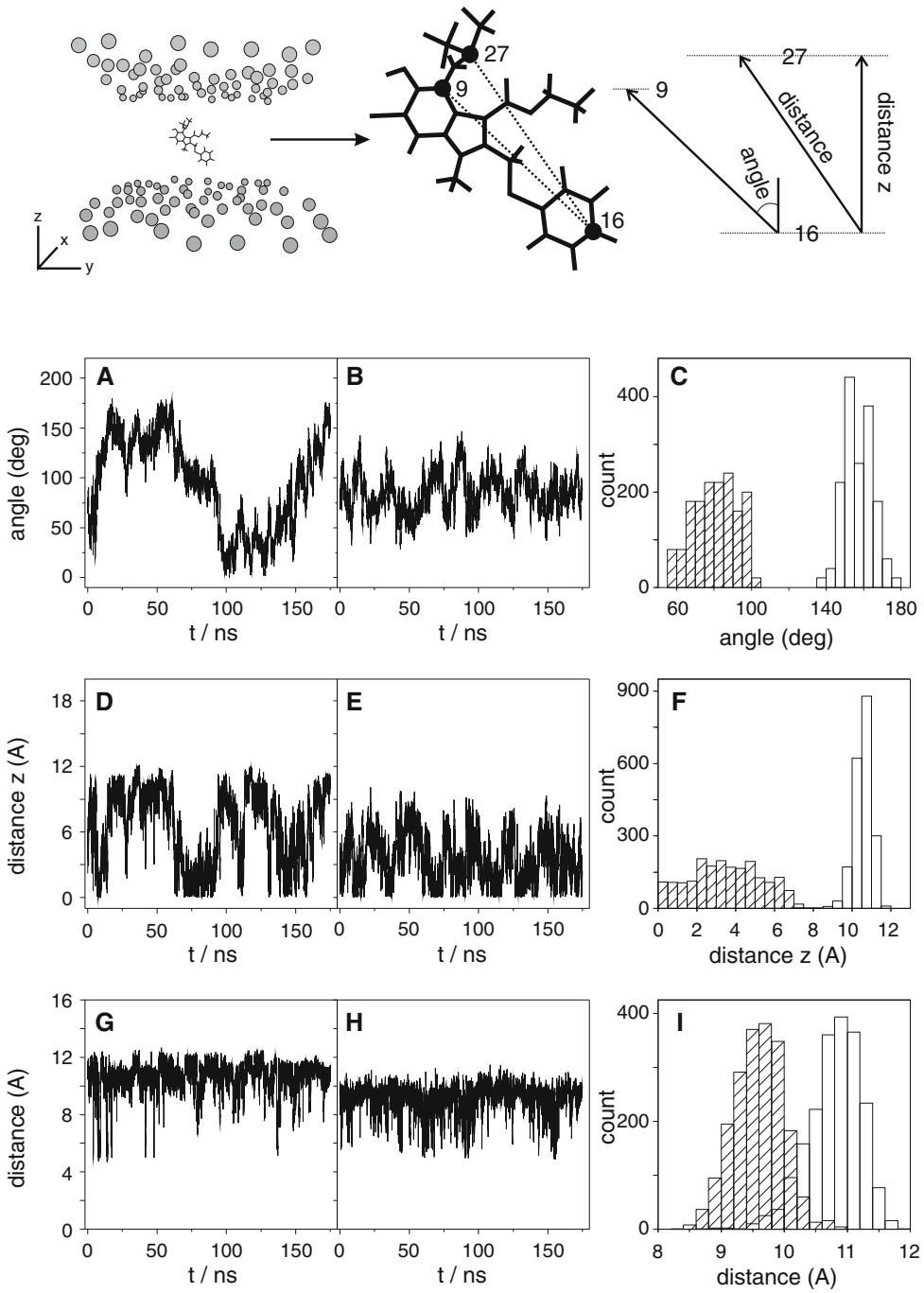

Fig. 3 Time variation of the (**a**, **b**) angle defined by the vector joining atoms 9 and 16 of Arb (**a**) and Arp (**b**) and the membrane *z*-axis and the corresponding histogram plots for the last 2 ns (**c**). Time variation of the (**d**, **e**) distance difference defined by the *z*-axis values of atoms 27 and 16 of Arb (**d**) and Arp (**e**) and the corresponding histogram plots for the last 2 ns (**f**). Time variation of the (**g**, **h**) distance defined by the vector joining atoms 27 and 16 of Arb (**a**) and Arp (**b**) and the corresponding histogram plots for the last 2 ns (**i**). For the histogram plots, non-stripped bars correspond to Arb whereas stripped bars correspond to Arp. See text for details

existence of differences in the location of the phosphate atoms depending on phospholipid type. Furthermore, the location and/or orientation of Arp in the bilayer induced a larger distortion on the phosphate atoms of the phospholipids than Arb. This can be easily observed on the of the Arb/Arp mass density profile expansion shown on Fig. 4e. The Arb mass density profile is a broad one, with a half bandwidth of about 9.35 Å, whereas the mass density profile half bandwidth of Arp is about 6.4 Å. This data show us that the orientation of Arp in the membrane is nearly parallel to the membrane *z*-axis, whereas Arp tends to be perpendicular to it. This difference in molecule location and orientation in the membrane is the cause of the different effects commented above.

We have also studied the effect of the presence of both Arb and Arp molecules on the hydrocarbon chain order for the phospholipid acyl chains (Figure S2). With that aim, we have obtained the deuterium order parameter, $-S_{CD}$, for the saturated and unsaturated hydrocarbon acyl chains of both POPC and POPG phospholipids in the POPC/POPG/Chol/

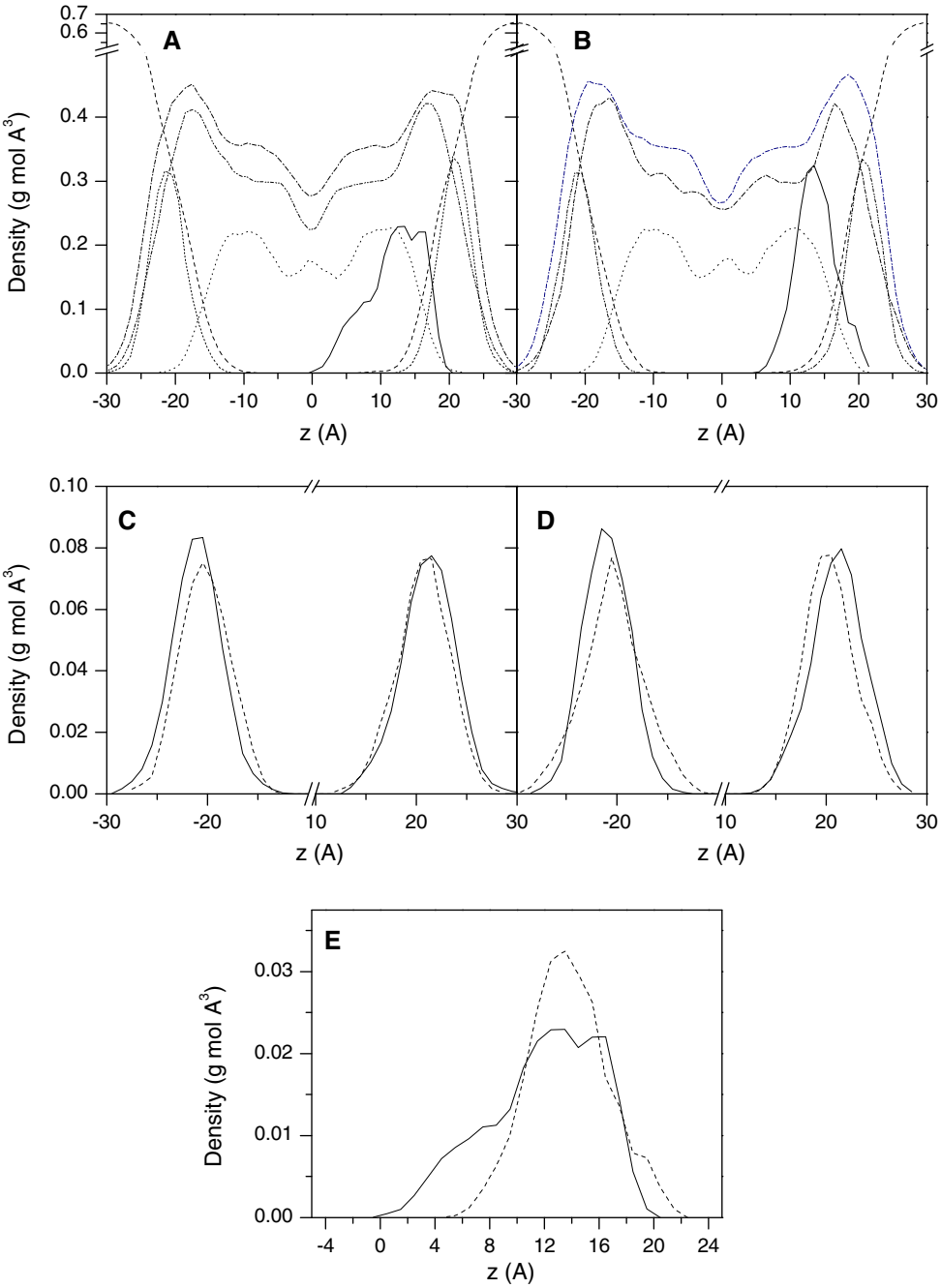

Fig. 4 Mass density profiles for the last 5 ns of the simulation for systems composed of POPC/POPG/Chol/Arb (**a**) and POPC/POPG/Chol/Arp (**b**). The density profiles corresponding to Arb/Arp (——, multiplied by 10), POPC and POPG (—·—, POPG multiplied by 2), Chol (···, multiplied by 3), water (**---**), and phospholipid phosphate atoms (—···—, multiplied by 3) are shown. Expansion of the mass density profile of the (**c**, **d**) phosphate atoms of POPC (——) and POPG (**---**, multiplied by 2) for the **c** POPC/POPG/Chol/Arb and **d** POPC/POPG/Chol/Arp systems, and **e** superposition of the mass density profile corresponding to Arb (——) and Arp (**---**) in each individual system

Arb and POPC/POPG/Chol/Arp systems. When there is full order along the normal bilayer, $-S_{CD}$ has a value of 0.5, but when there is full order along the bilayer plane, $-S_{CD}$ has a value of −0.25 (Tieleman et al. 1997). An isotropic orientation is given by a $-S_{CD}$ value of 0.

The average $-S_{CD}$ values of the sn-1 and sn-2 acyl chains of POPC for the POPC/POPG/Chol/Arb system are relatively similar in both leaflets, z+ and z− (Fig. S2A and S2B, respectively), in agreement with the profiles observed earlier for experimental and simulated data (Bockmann et al. 2003; Klauda et al. 2010; Tsai et al. 2015). The same can be said for the average $-S_{CD}$ values of the sn-1 of POPG in the same system (Fig. S2E). However, small but significant differences could be observed for the $-S_{CD}$ values of the sn-2 of POPG when comparing leaflets z+ and z− (Fig. S2F), indicating that Arb modifies the order parameter of the hydrocarbon chains in the leaflet it resides. Since there is only one molecule of Arb per system, we have also calculated the $-S_{CD}$ values of the hydrocarbon acyl chains of POPC and POPG molecules that are within 7 Å of the molecule of Arb. The presence of Arb gives place to minor differences in the $-S_{CD}$ values, particularly on carbons 5–10 of the sn-1 chain of POPC (Fig. S2A),

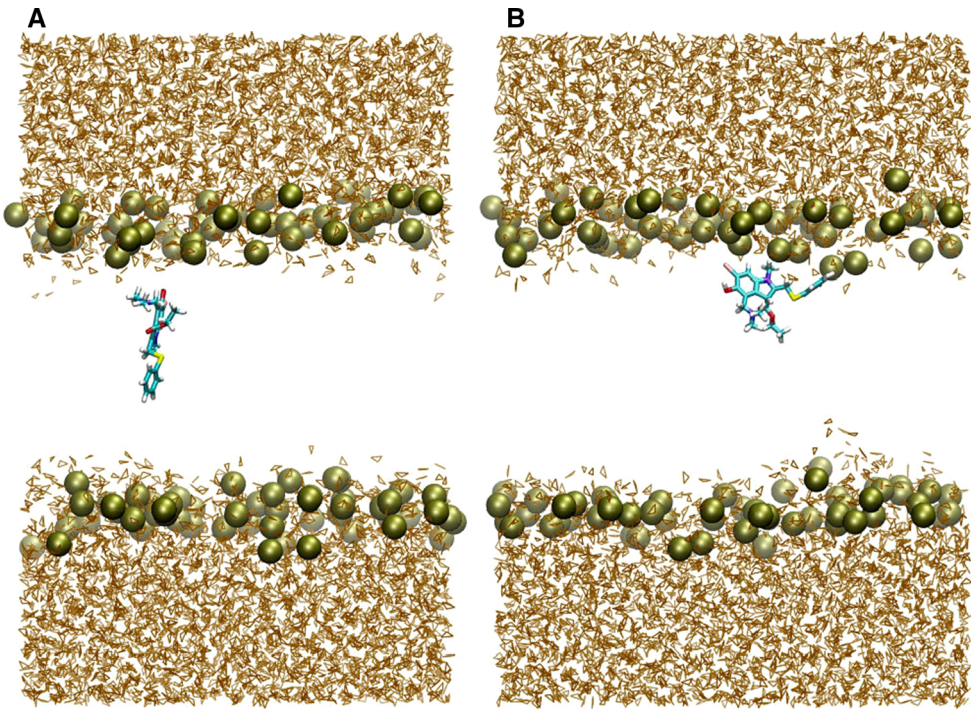

Fig. 5 Final ($t = 175$ ps) snapshots of the systems **a** POPC/POPG/Chol/Arb and **b** POPC/POPG/Chol/Arp membrane model systems. The phospholipid and water molecules are shown in ocher. The Arb/Arp molecules and the phospholipid phosphate atoms are depicted in licorize and VDW drawing styles, respectively. The phospholipid and cholesterol molecules have been removed for clarity

10–14 of the sn-1 chain of POPG (Fig. S2E), and 12–16 of the sn-2 chain of POPG (Fig. S2F).

Similarly to what has been said for the $-S_{CD}$ values of POPC in the POPC/POPG/Chol/Arb system, the average $-S_{CD}$ values of the sn-1 and sn-2 acyl chains of POPC in the POPC/POPG/Chol/Arp system were relatively similar in both leaflets, z+ and z− (Fig. S2C and S2D, respectively). The $-S_{CD}$ values of the sn-1 and sn-2 acyl chains of POPC molecules that are within 7 Å of the molecule of Arb are similar to the global $-S_{CD}$ values (Fig. S2C and S2D). There were no significant differences between the $-S_{CD}$ values of POPG in the POPC/POPG/Chol/Arp system of both leaflets z+ and z−, either in the sn-1 chain or in the sn-2 one (Fig. S2G and S2H). However, differences in the $-S_{CD}$ values of POPG within 7 Å of the molecule of Arp could be observed, more apparent on the sn-1 chain than on the sn-2 one. As observed in Fig. S2G, carbons 3–13 of the sn-1 chain have greatly reduced $-S_{CD}$ values when compared to the global $-S_{CD}$ values, indicating the specific interaction of Arp with the sn-1 chain of POPG. Although some differences were observed for the sn-2 chain of POPG, these were not as significant as those observed for the sn-1 chain (compare Fig. 3g, h).

Conclusions

Arbidol, incorporates rapidly into model and biological membranes, intercalates in the phospholipid palisade structure of the membrane and modifies the physicochemical properties of membrane phospholipids (Teissier et al. 2011b; Villalain 2010). In this work, we have studied the location and orientation of arbidol in the membrane by molecular dynamics simulations. The final configurations for both POPC/POPG/Chol/Arb and POPC/POPG/Chol/Arp membrane model systems are shown in Fig. 5a, b. At the start of the simulation, both Arb/Arp molecules were located in the middle of the palisade structure of the bilayer and at the same coordinates. At the end of the simulation, Arb locates in the middle of the palisade structure of the monolayer in a perpendicular orientation to the membrane surface. However, Arp locates near the surface in vicinity to the phospholipid interfacial region and nearly parallel to the membrane surface. Therefore, both Arb and Arp tend to locate preferentially in a definite part of the membrane, with a specific and completely different orientation. The different disposition of both molecules in the membrane could differently perturb the membrane structure depending on the relative proportion of the protonated and unprotonated forms in the membrane. Moreover, since Arp, positively charged, seems to interact stronger with POPG, negatively charged, than with POPC, it would be possible that the active molecule of arbidol in the membrane would be the protonated positively charged molecule. The broad antiviral activity of arbidol would rely on the effects it exerts on the membrane structure in general and in negatively charged phospholipids in particular.

Acknowledgments The research conducted in this work was partially funded by grant BFU2013-43198-P (Ministerio de Economía y

Competitividad, Spain) to J.V. NAMD was developed by the Theoretical and Computational Biophysics Group in the Beckman Institute for Advanced Science and Technology at the University of Illinois at Urbana-Champain.

Compliance with Ethical Standards

Conflict of interest None to declare.

References

Anézo C, de Vries AH, Höltje H-D, Tieleman DP, Marrink S-J (2003) Methodological issues in lipid bilayers simulations. J Phys Chem B 107:9424–9433

Blaising J, Polyak SJ, Pecheur EI (2014) Arbidol as a broad-spectrum antiviral: an update. Antiviral Res 107:84–94

Bockmann RA, Hac A, Heimburg T, Grubmuller H (2003) Effect of sodium chloride on a lipid bilayer. Biophys J 85:1647–1655

Boriskin YS, Leneva IA, Pecheur EI, Polyak SJ (2008) Arbidol: a broad-spectrum antiviral compound that blocks viral fusion. Curr Med Chem 15:997–1005

Brooks MJ, Burtseva EI, Ellery PJ, Marsh GA, Lew AM, Slepushkin AN, Crowe SM, Tannock GA (2012) Antiviral activity of arbidol, a broad-spectrum drug for use against respiratory viruses, varies according to test conditions. J Med Virol 84:170–181

Delogu I, Pastorino B, Baronti C, Nougairede A, Bonnet E, de Lamballerie X (2011) In vitro antiviral activity of arbidol against Chikungunya virus and characteristics of a selected resistant mutant. Antiviral Res 90:99–107

Deng HY, Luo F, Shi LQ, Zhong Q, Liu YJ, Yang ZQ (2009) Efficacy of arbidol on lethal hantaan virus infections in suckling mice and in vitro. Acta Pharmacol Sin 30:1015–1024

Feller SE, Zhang Y, Pastor RWJ (1995) Constant pressure molecular dynamics simulation: the Langevin piston method. J Chem Phys 103:4613–4621

Galiano V, Villalain J (2015) Oleuropein aglycone in lipid bilayer membranes. A molecular dynamics study. Biochim Biophys Acta 1848:2849–2858

Giorgino T (2014) Computing 1-D atomic densities in macromolecular simulations: the density profile tool for VMD. Comput Phys Commun 185:317–322

Guixa-Gonzalez R, Rodriguez-Espigares I, Ramirez-Anguita JM, Carrio-Gaspar P, Martinez-Seara H, Giorgino T, Selent J (2014) MEMBPLUGIN: studying membrane complexity in VMD. Bioinformatics 30:1478–1480

Humphrey W, Dalke A, Schulten K (1996) VMD: visual molecular dynamics. J Mol Graph 14(33–8):27–28

Ingolfsson HI, Melo MN, van Eerden FJ, Arnarez C, Lopez CA, Wassenaar TA, Periole X, de Vries AH, Tieleman DP, Marrink SJ (2014) Lipid organization of the plasma membrane. J Am Chem Soc 136:14554–14559

Kandt C, Ash WL, Tieleman DP (2007) Setting up and running molecular dynamics simulations of membrane proteins. Methods 41:475–488

Klauda JB, Venable RM, Freites JA, O'Connor JW, Tobias DJ, Mondragon-Ramirez C, Vorobyov I, MacKerell AD Jr, Pastor RW (2010) Update of the CHARMM all-atom additive force field for lipids: validation on six lipid types. J Phys Chem B 114: 7830–7843

Kosinova P, Berka K, Wykes M, Otyepka M, Trouillas P (2012) Positioning of antioxidant quercetin and its metabolites in lipid bilayer membranes: implication for their lipid-peroxidation inhibition. J Phys Chem B 116:1309–1318

Leneva IA, Russell RJ, Boriskin YS, Hay AJ (2009) Characteristics of arbidol-resistant mutants of influenza virus: implications for the mechanism of anti-influenza action of arbidol. Antiviral Res 81:132–140

Liu Q, Xiong HR, Lu L, Liu YY, Luo F, Hou W, Yang ZQ (2013) Antiviral and anti-inflammatory activity of arbidol hydrochloride in influenza A (H1N1) virus infection. Acta Pharmacol Sin 34:1075–1083

Martyna GJ, Tobias DJ, Klein ML (1994) Constant pressure molecular dynamics algorithms. J Chem Phys 101:4177–4189

Murzyn K, Rog T, Jezierski G, Takaoka Y, Pasenkiewicz-Gierula M (2001) Effects of phospholipid unsaturation on the membrane/water interface: a molecular simulation study. Biophys J 81: 170–183

Nasser ZH, Swaminathan K, Muller P, Downard KM (2013) Inhibition of influenza hemagglutinin with the antiviral inhibitor arbidol using a proteomics based approach and mass spectrometry. Antiviral Res 100:399–406

Ozu M, Alvarez HA, McCarthy AN, Grigera JR, Chara O (2013) Molecular dynamics of water in the neighborhood of aquaporins. Eur Biophys J 42:223–239

Patra M, Karttunen M, Hyvonen MT, Falck E, Lindqvist P, Vattulainen I (2003) Molecular dynamics simulations of lipid bilayers: major artifacts due to truncating electrostatic interactions. Biophys J 84:3636–3645

Pecheur EI, Lavillette D, Alcaras F, Molle J, Boriskin YS, Roberts M, Cosset FL, Polyak SJ (2007) Biochemical mechanism of hepatitis C virus inhibition by the broad-spectrum antiviral arbidol. Biochemistry 46:6050–6059

Pecheur EI, Borisevich V, Halfmann P, Morrey JD, Smee DF, Prichard M, Mire CE, Kawaoka Y, Geisbert TW, Polyak SJ (2016) The synthetic antiviral drug arbidol inhibits globally prevalent pathogenic viruses. J Virol. doi:10.1128/JVI.02077-15

Perfetto B, Filosa R, De Gregorio V, Peduto A, La Gatta A, de Caprariis P, Tufano MA, Donnarumma G (2014) In vitro antiviral and immunomodulatory activity of arbidol and structurally related derivatives in herpes simplex virus type 1-infected human keratinocytes (HaCat). J Med Microbiol 63:1474–1483

Phillips JC, Braun R, Wang W, Gumbart J, Tajkhorshid E, Villa E, Chipot C, Skeel RD, Kale L, Schulten K (2005) Scalable molecular dynamics with NAMD. J Comput Chem 26:1781–1802

Shi L, Xiong H, He J, Deng H, Li Q, Zhong Q, Hou W, Cheng L, Xiao H, Yang Z (2007) Antiviral activity of arbidol against influenza A virus, respiratory syncytial virus, rhinovirus, coxsackie virus and adenovirus in vitro and in vivo. Arch Virol 152:1447–1455

Teissier E, Penin F, Pecheur EI (2011a) Targeting cell entry of enveloped viruses as an antiviral strategy. Molecules 16:221–250

Teissier E, Zandomeneghi G, Loquet A, Lavillette D, Lavergne JP, Montserret R, Cosset FL, Bockmann A, Meier BH, Penin F, Pecheur EI (2011b) Mechanism of inhibition of enveloped virus membrane fusion by the antiviral drug arbidol. PLoS ONE 6:e15874

Tieleman DP, Marrink SJ, Berendsen HJ (1997) A computer perspective of membranes: molecular dynamics studies of lipid bilayer systems. Biochim Biophys Acta 1331:235–270

Tsai HH, Lee JB, Li HS, Hou TY, Chu WY, Shen PC, Chen YY, Tan CJ, Hu JC, Chiu CC (2015) Geometrical effects of phospholipid olefinic bonds on the structure and dynamics of membranes: a molecular dynamics study. Biochim Biophys Acta 1848:1234–1247

van Meer G, Voelker DR, Feigenson GW (2008) Membrane lipids: where they are and how they behave. Nat Rev Mol Cell Biol 9:112–124

Vanommeslaeghe K, Hatcher E, Acharya C, Kundu S, Zhong S, Shim J, Darian E, Guvench O, Lopes P, Vorobyov I, Mackerell AD Jr (2010) CHARMM general force field: a force field for drug-like

molecules compatible with the CHARMM all-atom additive biological force fields. J Comput Chem 31:671–690

Villalain J (2010) Membranotropic effects of arbidol, a broad anti-viral molecule, on phospholipid model membranes. J Phys Chem B 114:8544–8554

Wu EL, Cheng X, Jo S, Rui H, Song KC, Davila-Contreras EM, Qi Y, Lee J, Monje-Galvan V, Venable RM, Klauda JB, Im W (2014) CHARMM-GUI Membrane Builder toward realistic biological membrane simulations. J Comput Chem 35:1997–2004

Zhong Q, Yang Z, Liu Y, Deng H, Xiao H, Shi L, He J (2009) Antiviral activity of Arbidol against Coxsackie virus B5 in vitro and in vivo. Arch Virol 154:601–607

Zhuang X, Makover JR, Im W, Klauda JB (2014) A systematic molecular dynamics simulation study of temperature dependent bilayer structural properties. Biochim Biophys Acta 1838:2520–2529